

Reducing RES Droughts through the integration of wind and PV

Boris Morin, Damian Flynn, Aina Maimó Far, Conor Sweeney

November 29, 2024

Abstract

The dependence of renewable energy sources (RES) such as wind and photovoltaic (PV) systems on the weather poses a critical challenge for energy systems. This study investigates the impact of targeting a balanced distribution of wind and PV capacity on reducing periods of low renewable generation, known as RES droughts. Three different RES models are used to estimate the capacity factors for different installed capacities of wind and PV. The skill of the RES models is quantified by comparing capacity factor time series to observed data. Their skill at representing RES droughts is also quantified. The RES models are used to generate a 45-year hourly time series of RES generation, enabling analysis of the frequency, duration and return periods of RES droughts at a climatological scale. Results show the importance of using an accurate, validated RES model for RES drought risk assessment. The addition of PV capacity to a wind-dominated system results in a large reduction in the frequency and duration of RES droughts, as well as reducing seasonal drought patterns. These findings underscore the importance of diversification in RES capacity to enhance energy security and resilience.

Keywords: RES Drought, Wind Power, Solar PV Power, Renewable Energy Sources, Return Periods

1 Introduction

The EU aims to generate at least 69% of its electricity from renewable energy sources (RES) by 2030, up from 41% in 2022 [2]. While this transition is essential for reducing greenhouse gas emissions, it also highlights the challenge of managing the variability of weather-dependent energy sources like wind and photovoltaic (PV) power. This challenge is compounded by the increasing electrification of energy sectors, which places greater demand on the power system and makes it more sensitive to meteorological conditions [3, 4, 5]. Periods of low renewable generation, known as *Dunkelflaute* or RES droughts, pose significant risks to grid stability and energy security, emphasizing the need for a resilient energy system to meet both growing electricity demand and decarbonization targets.

This study focuses on Ireland, a region with a strong reliance on wind energy, which has ambitious targets for PV expansion. This case study provides valuable insights into the potential benefits of diversifying the renewable energy mix on RES droughts. The performance of different RES models are compared, and a 45-year time series of RES generation is produced. The results highlight the role of increased PV capacity in reducing RES drought risks, offering insights for policymakers and energy planners.

For this study, a RES drought event is defined as occurring when the average capacity factor (CF) remains below a fixed threshold for a given duration, following the methodology used in other research [6, 7, 8, 9]. Alternative methods exist for defining RES droughts. One approach

uses relative CF thresholds that change over the year to account for seasonal variations in renewable energy generation [10, 11, 12, 13, 14]. Another common method relies on percentile-based thresholds, where drought events are defined by identifying periods of unusually low generation relative to historical production levels, typically based on the lowest production percentiles [15, 13]. Additionally, some studies combine these definitions with metrics that incorporate the demand side of energy consumption, analysing the balance between supply and demand during drought periods [10, 11, 13, 15]. In this paper, the focus is exclusively on energy generation, and a fixed threshold approach to define RES droughts is used, which facilitates consistent inter-comparison between scenarios with different installed wind and PV capacities.

RES droughts are identified using wind and PV CF time series. In this study, three different datasets are used, all of which are driven by ERA5 data [16]. Two of the datasets are part of C3S Energy (C3S-E) [17], an energy-based operational dataset produced by the EU Copernicus Climate Change Service [18]. One of the C3S-E datasets provides CF time series aggregated at the national scale, while the other provides the CF time series at each grid point, at the ERA5 resolution of 0.25° . The third dataset was generated using the Atlite model [19], which converts the ERA5 atmospheric data to a generation time series using specified wind turbine and PV panel models. Atlite is an open-source tool developed by PyPSA [19] and is widely used for estimating wind and PV generation [8, 20, 21, 22].

The datasets used in this study are detailed in section 2, which describes their characteristics and relevance for evaluating RES droughts. Section 3 outlines the RES models used to simulate wind and PV generation and provides the methodology for defining and identifying RES drought events, including the thresholds and metrics applied. In section 4, the models are first verified against observed energy data to assess their accuracy, followed by an analysis of RES drought occurrences for two scenarios with different ratios of installed wind to PV capacities. Finally, section 5 offers a discussion of the results in the context of energy reliability and future planning, followed by the main conclusions and recommendations for further research.

2 Data

This study uses publicly available datasets to construct and validate the models for estimating the CF of wind and PV energy. The primary data sources include: EirGrid, the transmission system operator (TSO) for the Republic of Ireland; the ERA5 reanalysis dataset; and the C3S-E datasets.

2.1 Wind and PV Generation & Capacity

EirGrid, the TSO for the Republic of Ireland, and SONI, the Northern Ireland TSO, provide detailed datasets on all wind and PV farms across the island of Ireland (Republic of Ireland and Northern Ireland) from 1990 to the present [23]. These datasets include information such as each farm’s installed capacity, name, and connection date. To enhance the accuracy of this data, the longitude and latitude for each farm were manually determined through online searches. For simplicity, this data will be referred to as originating from EirGrid, as all-island data was directly obtained from EirGrid, and the combined regions of the Republic of Ireland and Northern Ireland will be referred to as Ireland throughout the remainder of this document.

The spreadsheet available from the EirGrid website contains two key variables: generation and availability. Generation is the energy that a RES farm actually contributed to the grid, which may include limitations introduced by the TSO to maintain grid stability, such as constraints

and curtailment. Availability represents the energy that would have been generated from a RES farm if no grid constraints had been applied, making it representative of the weather-related response. Generation and availability values are available from 2014 onward for wind and from 2018 onward for PV, although PV only became present in the Republic of Ireland data in 2023. Availability values are used to calculate the skill of the RES models.

2.2 Atmospheric Variables

Atlite and C3S-E datasets are driven by the ERA5 reanalysis [16], produced by the European Centre for Medium-Range Weather Forecasts (ECMWF). This global gridded dataset provides hourly atmospheric variables from 1940 to the present at a horizontal resolution of 0.25° , which is approximately every 27 km. It is widely used for estimating PV and wind energy [8, 18, 24, 25]. Table 1 lists the ERA5 variables used by Atlite and C3S-Energy.

ERA5 name	variable
100 metre zonal and meridional wind speed	u_{100}, v_{100}
2 metre temperature	$t2m$
Surface net solar radiation	ssr
Surface solar radiation downwards	$ssrd$
Top of atmosphere incident radiation	$tisr$
Total sky direct solar radiation at surface	$fdir$

Table 1: ERA5 variables used to calculate wind and PV generation.

2.3 C3S Energy

The EU Copernicus Climate Change Service developed the C3S-E renewable energy dataset for Europe [18], using ERA5 atmospheric variables and weather-to-energy models. This dataset provides hourly CF for wind and PV energy from 1979 to the present. The data are available on the same grid as the ERA5 data, which has a horizontal resolution of 0.25° . The time series are also available for download at two aggregated scales: regional (NUTS 2) and national.

The C3S-E dataset estimates wind energy using wind speeds at 100 metres (u_{100}, v_{100}) and a standard turbine model, the Vestas V136/3450, with a fixed hub height of 100 m. This choice is based on expert advice and the trend in wind turbine installation. The PV generation model used by C3S-E uses two ERA5 variables: Surface solar radiation downwards ($ssrd$) and air temperature ($t2m$). PV generation is calculated multiple times, using the same model with different azimuth and tilt angles. The results are aggregated based on a statistical distribution of the module angles based on the geographical location [26].

3 Methods

This study uses three datasets to analyse RES droughts across the island of Ireland. Data downloaded from C3S-E were used to obtain two datasets: one based on national-level data (C3S-E N), and another on grid-level data (C3S-E G). The third dataset was computed using the Atlite model (Atlite).

3.1 C3S-Energy National

For national-level analyses, the aggregated CF time series provided by C3S-E were used at two levels: Republic of Ireland (NUTS0: IE) and Northern Ireland (NUTS2: UKN0). These are based on the assumption by C3S-E that RES generation occurs at every ERA5 grid point in Ireland. We computed a weighted average of these, based on the installed capacity of each one, to represent the total CF for Ireland.

3.2 C3S-E Gridded

The gridded dataset from C3S-E was used to create CF datasets which account for the location of RES farms in Ireland. A list of the RES farms in Ireland was compiled, including each farm's latitude, longitude and installed capacity. Using these coordinates, the nearest grid point on the C3S-E grid was identified for each farm. The CF values from the C3S-E dataset corresponding to these grid points were retrieved. A weighted average of the CF values was calculated, with the installed capacity of each farm serving as the weight, to construct the CF time series for Ireland. This process resulted in a time series of RES generation for each energy source (wind and PV) for Ireland, which takes the location of the RES farms into account.

3.3 Atlite

Atlite transforms weather data into energy data using the gridded ERA5 data and the locations of existing RES farms, as described in C3S-E G. ERA5 data for wind speed at 100 metres (u_{100} , v_{100}) are used to calculate wind generation, while the ERA5 irradiance variables (ssr , $ssrd$, $tisr$, and $fdir$) and air temperature ($t2m$) are used to calculate PV generation. A key distinction between C3S-E and Atlite lies in their representation of wind turbines and PV panels. This study identifies the most appropriate wind turbine power curve to use from the 121 power curves made available by Renewables.ninja [27]. The selection of a specific wind turbine and PV panel characteristics is further discussed and explained in section 4.1.

3.4 Energy Scenarios

In addition to analysing wind and PV generation separately, a combined CF was computed for each model by averaging wind and PV generation, weighted by their installed capacities at the end of 2023 (6.7 GW for wind and 0.6 GW for PV). Given that PV capacity in Ireland is low in 2023, and to explore how a more balanced distribution of wind and PV might impact RES droughts, this study also considered a balanced scenario, where the installed PV capacity is assumed to increase to 8 GW, while wind capacity rises to 9 GW. These values are based on targets outlined in the roadmap published by EirGrid and SONI [29]. New time series were generated for both the Atlite and C3S-E G PV models, incorporating a revised distribution of installed capacity across Ireland as specified in the roadmap. For wind, the CF time series remains unchanged, as significant shifts in the location of wind farms are not expected. The PV and wind time series were then combined using updated weights that reflect the installed capacities in the balanced scenario (9 GW for wind and 8 GW for PV).

In total, twelve CF time series were analysed in this study, six for individual wind and PV CF (three models for each source) in the existing scenario, and an additional six time series that include the combined CF for both existing and balanced scenarios across the different models.

This approach allows for a comparative analysis between a wind-dominated system (the existing scenario) and a more evenly distributed system (the balanced scenario), assessing how the balance of RES capacity affects the occurrence of RES droughts.

3.5 RES Drought Definition

In this study, a RES drought event was defined as occurring when the 24-hour moving average of CF remains below a fixed threshold of 0.1 for a period of longer than 24 hours. The choice of this threshold is somewhat arbitrary, but aligns with similar studies on low renewable energy production [6, 7, 9]. By using a 24-hour moving average, fewer but longer-lasting events were captured compared to using the raw CF time series, which can be more sensitive to short-term fluctuations. A fixed threshold approach was chosen in this study to enable consistent inter-comparison between datasets.

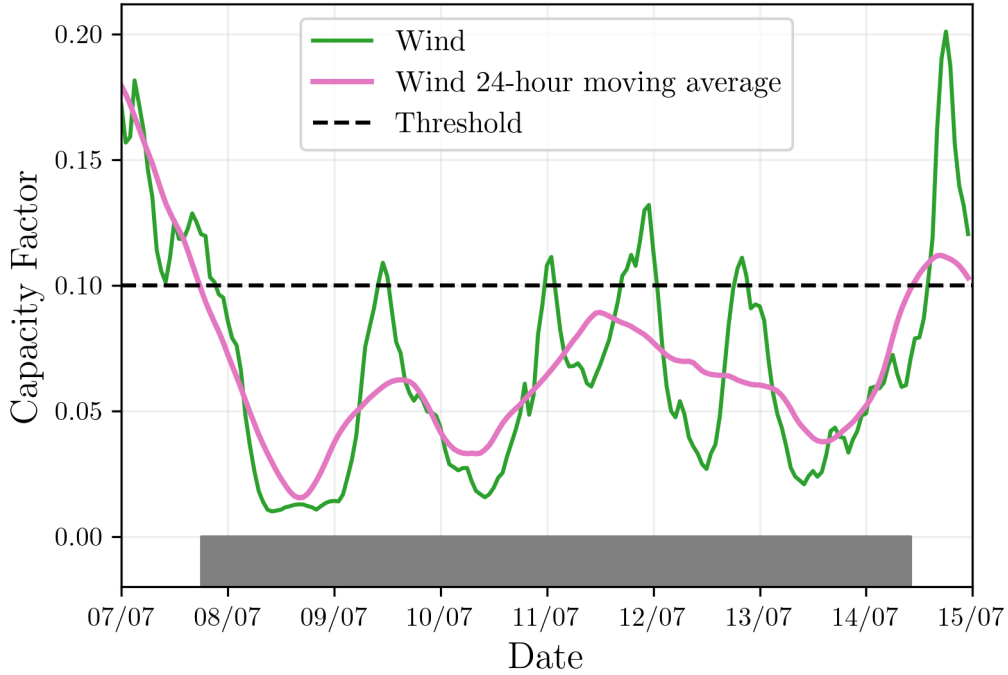


Figure 1: Wind time series of CF (green) and its 24-hour moving average (pink) from the 7th to the 15th of July 2021. The black dashed line indicates the CF threshold. The grey bar shows the period identified as a wind drought under our definition

The moving average approach smooths out short-term fluctuations, so that brief periods above the threshold do not interrupt an otherwise continuous low-CF period (Fig. 1). This means that a single hour above the threshold does not “break” a drought event if it is surrounded by prolonged low-generation hours. As a result, fewer but longer-lasting drought events are identified, which may better reflect real-world conditions where energy supply constraints persist over extended periods.

4 Results

4.1 Verification

The accuracy of the datasets used in this study was verified, before continuing to the analysis of RES droughts. For the verification process, time-varying values of installed capacity were used to account for changes in RES development over the verification period. This step allowed us to assess how well the datasets represent the production of renewable energy by comparing them against observed data.

4.1.1 Wind Energy

The C3S-E datasets use the Vestas V136/3450 wind turbine power curve, (Fig. 2a). The Atlite model allows the user to specify the power curve. We considered the 121 power curves available for download from Renewables.ninja [27]. For each power curve, Renewables.ninja also provides four associated smoothed power curves. The smoothing is done using a Gaussian filter with different standard deviations that depend on the wind speed. A separate wind CF time series for Ireland was generated for each of the wind turbine power curves and smoothing levels. The performance of each CF time series was then assessed based on four skill scores: correlation coefficient (CC), root mean square error (RMSE), mean bias error (MBE), and area under the curve. The area under the curve was calculated from histograms of the hourly CF values for the most recent decade, 2014-2023. Based on these metrics, the most representative power curve for Ireland was the Enercon E112.4500 power curve with the $0.3w$ smoothing filter.

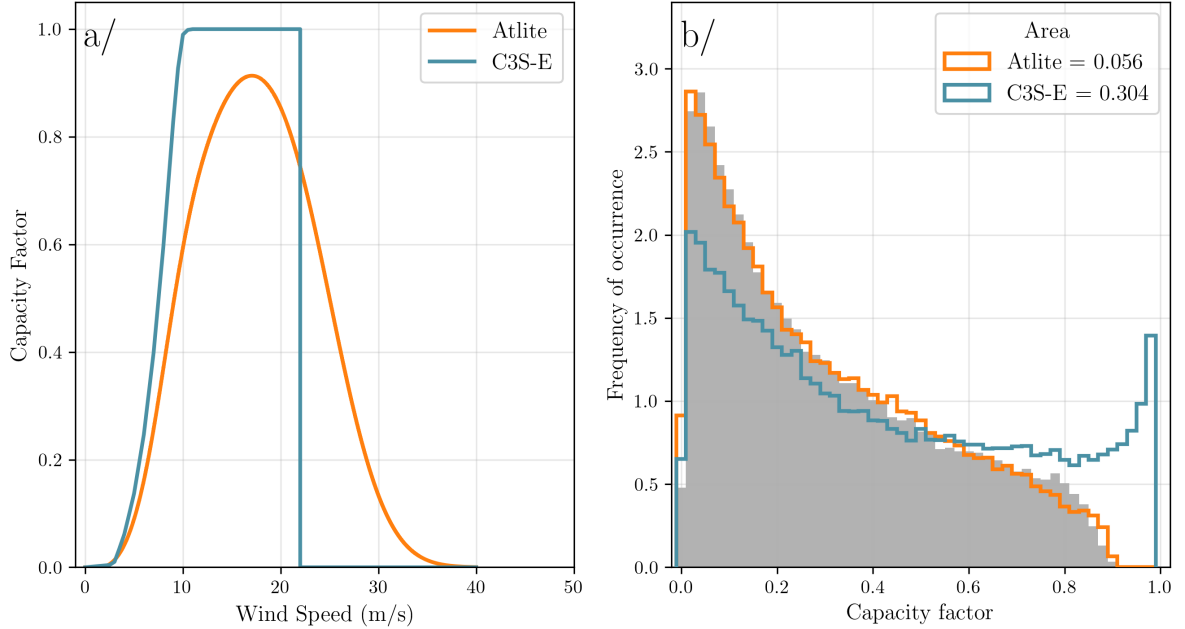


Figure 2: a/ Power curves of the Enercon E112.4500 with a 0.3 smoothing filter used by Atlite (orange) and the Vestas V136/3450 used by C3S-E (teal) b/ Histograms of wind CF for Ireland from Atlite (orange), C3S-E (teal) and EirGrid (shaded)

The smoothing of the wind turbine power curve represents losses associated with each turbine, as well as losses such as wake effects between turbines, which are important when modelling wind

energy on larger spatial scales. The histogram in Fig. 2b shows that the C3S-E power curve tends to underestimate low CF values and overestimate higher ones, whereas the smoothed Atlite power curve more closely follows the recorded wind availability data from EirGrid.

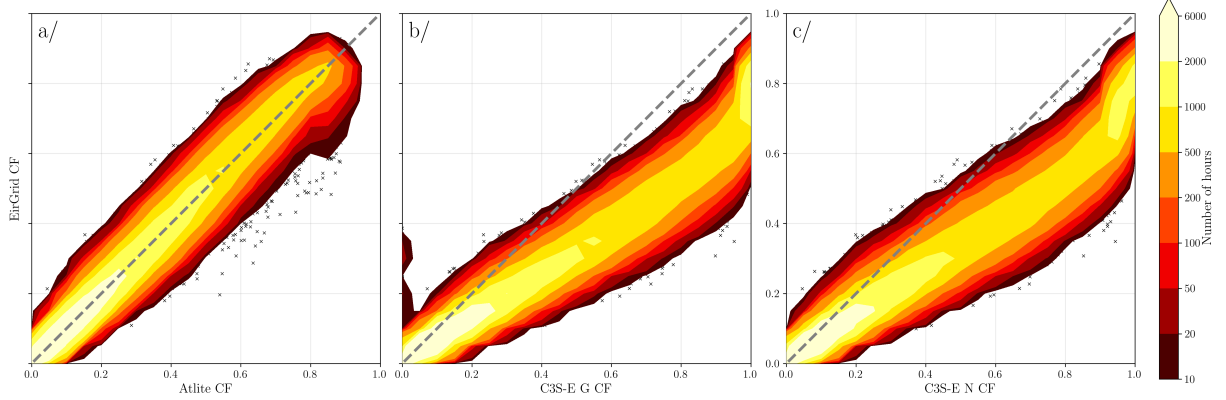


Figure 3: Wind CF density plot of the observed EirGrid CF (vertical axes) and modelled (horizontal axes) CF data for the Atlite (left panel), C3S-E G (central panel) and C3S-E N (right panel) models

The effect of the difference between the power curves is also visible in Fig. 3, which shows a density plot of wind CF values. The two C3S-E datasets are shown to overestimate the EirGrid CF, whereas the Atlite model is in good agreement with the EirGrid data. The skill scores presented in Table 2 show that Atlite performs better than the C3S-E datasets for all of the skill scores.

	Atlite	C3S-E G	C3S-E N
CC	0.981	0.972	0.970
RMSE	0.045	0.177	0.162
MBE	-0.003	0.137	0.121

Table 2: Skill scores for wind for the three datasets compared to EirGrid data

Fig. 4 presents results for the average annual number of wind drought events during the 2014 to 2023 validation period. The figure shows that Atlite shows the best agreement overall with the observed frequency and duration of wind drought events. This pattern is particularly evident for shorter-duration events, which are the most frequent.

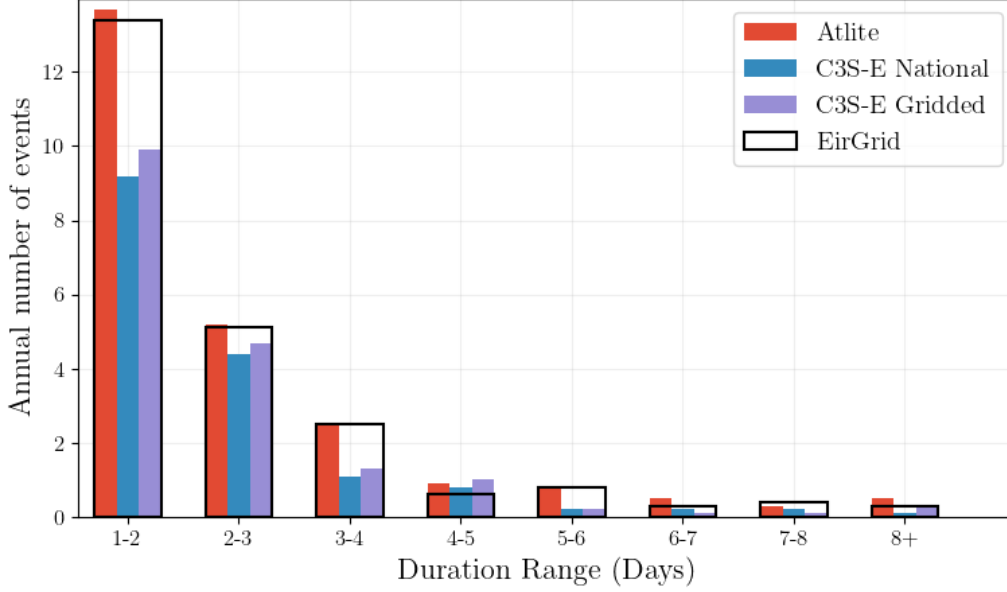


Figure 4: Average annual number of wind drought events for EirGrid (black), Atlite (red), C3S-E G (blue), and C3S-E N (purple)

4.1.2 PV Energy

The Atlite model allows the user to select certain PV panel characteristics. In this study, the three PV panel types available in the Atlite model were considered. Following the same methodology as in the previous section, the three available models were compared using four skill scores (CC, RMSE, MB, and area under the curve). Based on the best-performing metrics, the Breyer PV panel model was selected [28], using the Kaneka Hybrid panel option. For all PV farm locations, the azimuth angle is fixed at 180° (due south), and the optimal tilt angle option is applied.

The PV installed capacity available on the spreadsheets from EirGrid represents the Maximum Export Capacity (MEC) and does not accurately reflect the installed PV capacity. To enable actual PV generation potential to be modelled correctly, installed capacities were set at 1.4 times the MEC values. This installed capacity was used for PV generation, with farm output capped to the MEC value.

Figure 5 shows that the three datasets have a similar tendency to overestimate the CF compared to EirGrid, especially for high CF values. The skill scores presented in Table 3 indicate that C3S-E G performs best overall, with the lowest RMSE and a high correlation coefficient, suggesting a closer match to observed data. Atlite shows a slightly lower correlation and a higher RMSE, indicating larger deviations. All models show a slight positive bias, with Atlite exhibiting the most overestimation. These results reflect the broader challenges in accurately modelling PV, where variability is hard to capture. Nonetheless, C3S-E G's lower RMSE suggests it may be more reliable for PV CF modelling in this context.

Fig. 6 shows the number of PV drought events in 2023 across different duration ranges. The figure reveals partial agreement between the three datasets and the EirGrid data, with consistent results observed for duration ranges of 1-2, 3-4, 7-8, and 8+ days. However, discrepancies appear in the other ranges, where the models diverge from the EirGrid data. The main challenge in

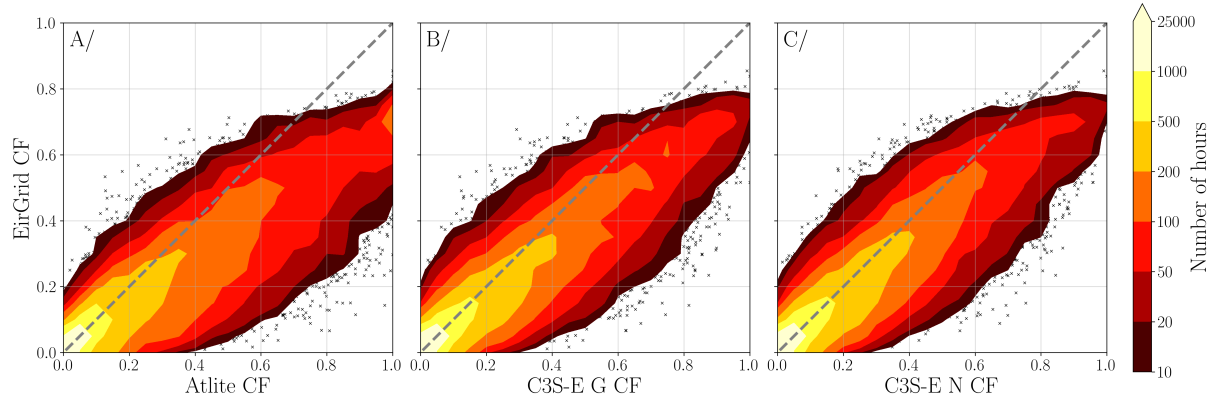


Figure 5: PV 2D density plot of the observed EirGrid (vertical axes) and modelled (horizontal axes) CF series for the Atlite (left panel), C3S-E G (central panel) and C3S-E N (right panel) models

	Atlite	C3S-E G	C3S-E N
CC	0.921	0.931	0.931
RMSE	0.119	0.090	0.113
MBE	0.046	0.027	0.021

Table 3: Skill scores for wind CF for the three datasets compared to EirGrid data

validating PV data stems from the recent installation of a large share of Ireland’s PV capacity, leading to uncertainties in PV generation data and the actual generating capacity in the first few months after each farm is connected. With over 65% of the total PV capacity installed in 2023, these data uncertainties significantly impact the ability to perform rigorous validation for PV drought events.

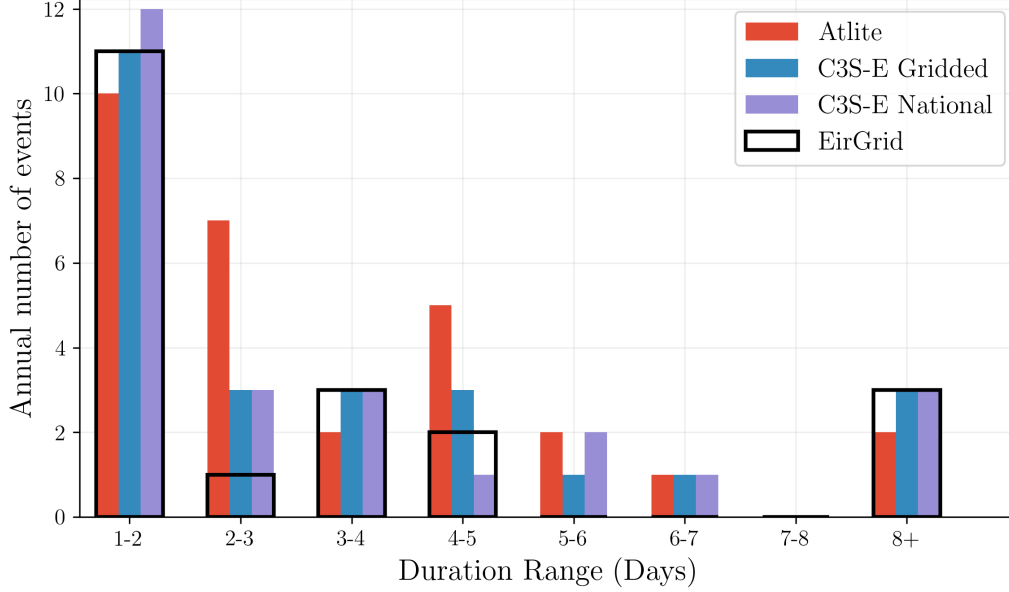


Figure 6: Annual number of PV drought events for EirGrid (black), Atlite (red), C3S-E G (blue), and C3S-E N (purple) in 2023

4.2 Analysis

In this section, RES drought events are evaluated under two different scenarios with fixed installed capacities: the existing scenario, with 89% of wind capacity (6.7 GW) and 11% of PV capacity (0.6 GW), and a balanced scenario, where wind capacity comprises 53% (9 GW) and PV capacity increases to 47% (8 GW). Both scenarios were driven by 45 years of ERA5 data. Using the RES drought identification process described in Section 3.5, wind and PV droughts are first analysed separately before presenting the results for combined (wind + PV) RES droughts under both scenarios.

4.2.1 Annual Number of RES Droughts

The first part of the analysis examines the annual number of RES drought events across the three datasets.

For wind (Fig. 7a), the number of events decreases as the duration range increases, with very few events lasting more than seven days. For PV (Fig. 7b), the number of events also declines as the duration range extends from one to eight days, followed by a slight increase for longer durations. This increase is due to extended low-generation periods occurring from November to March, depending on the dataset. When comparing wind and PV results (Fig. 7a & Fig. 7b), the median, first, and third quartiles for PV are consistently higher or equal to those for wind, across all duration ranges and datasets. This is due to the typically lower CF of PV compared to wind, especially in a region like Ireland where solar potential is limited. PV generation is also zero at night and constrained by the daily solar cycle, leading to a naturally higher frequency of RES droughts in PV compared to wind.

The bottom panels show the combination of wind and PV under the two capacity scenarios. In the existing RES installation scenario (Fig. 7c), the identified RES droughts closely match those

for wind alone, which is expected due to the dominance of installed wind capacity. In contrast, the balanced scenario (Fig. 7d) shows a clear reduction in the number of drought events across all datasets and durations, with a decrease of the total number of events of 56% for Atlite, 52% for C3S-E G, and 50% for C3S-E N. This reduction is attributed to the anti-correlation between wind and PV production throughout the year, a phenomenon well-documented in the literature [6].

The median, first, and third quartiles for the Atlite dataset are consistently greater than or equal to those of the other two datasets, regardless of the duration range or type of renewable energy considered. This difference arises from the wind turbine power curve model used in the C3S-E datasets, which tends to overestimate the wind CF (Fig. 3). As a result, the overall number of RES droughts is underestimated in the C3S-E datasets compared to Atlite.

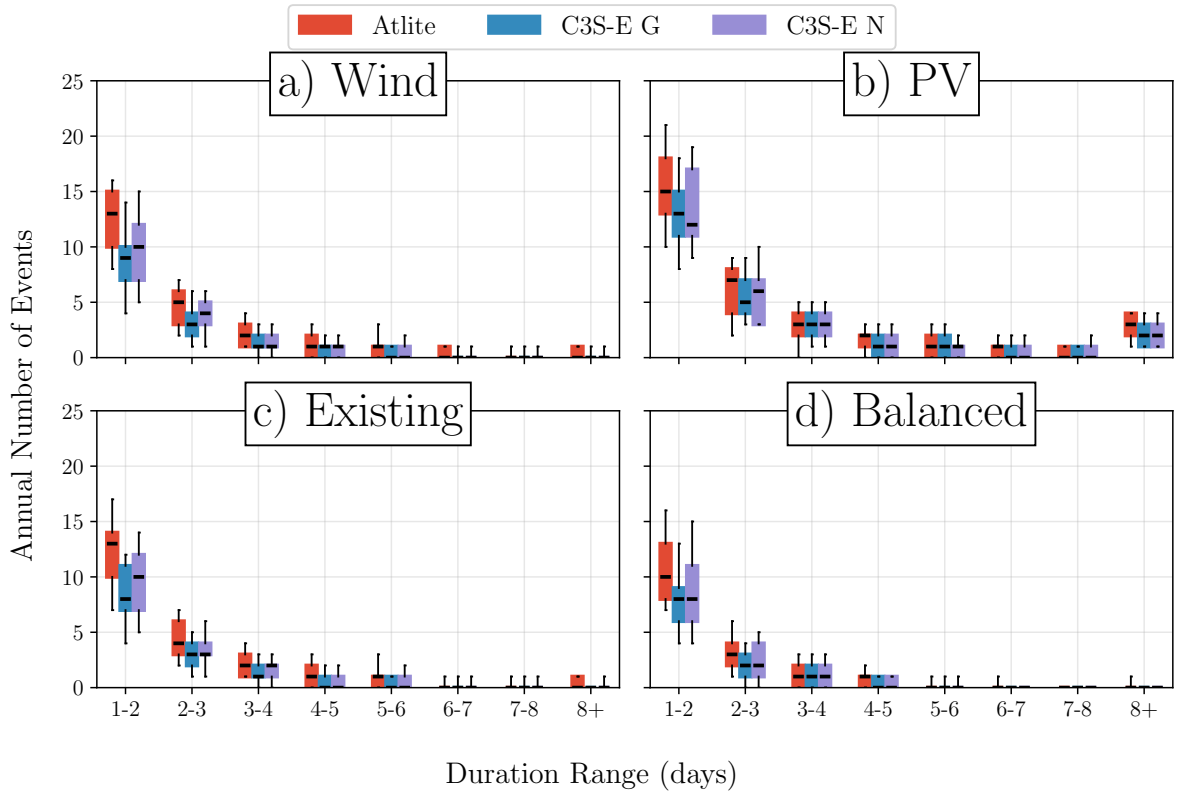


Figure 7: Annual number of RES droughts for a) Wind, b) PV, and the combination for the c) existing and d) balanced installed capacity for Atlite (red), C3S-E G (blue), and C3S-E N (purple). The x-axis represents duration ranges in days (lower bound included), while the y-axis indicates the annual number of events. The boxes display the first and third quartiles and the median is marked by a black line. The whiskers indicate the 5th and 95th percentiles

4.2.2 Return Periods of RES Drought Duration

The RES drought events identified over the 45-year period were used to calculate the return periods for different RES drought durations. A return period refers to the estimated average interval between occurrences of events with a specified duration or intensity. Fig. 8 illustrates the return periods for varying RES drought durations, highlighting how often different drought lengths are likely to occur across the datasets. This analysis provides insight into the frequency and likelihood of prolonged low-generation periods, which is crucial for evaluating the potential impact of RES droughts on energy reliability and security of supply.

For wind (Fig. 8a), the duration of RES droughts increases in a log-linear fashion across the three datasets. The log-linear trend indicates a predictable relationship between drought duration and occurrence, with longer RES droughts becoming exponentially less likely as duration increases.

For PV (Fig. 8b), Atlite behaves differently than the two C3S-E datasets. The Atlite results show a log-linear increase but reach higher values in general with the longest event lasting forty days. For C3S-E G and C3S-E N, the duration of RES droughts increases in a log-linear pattern for events lasting less than 16 days. Beyond this duration, there is a sharp rise in drought duration for events up to a one-year return period. This sudden increase reflects the impact of winter on PV generation in Ireland, as PV output often remains below the CF threshold for extended periods during winter months. The difference between Atlite and the C3S-E datasets arises from how each model handles PV output near the threshold of 0.1 CF. Atlite remains slightly above the threshold more frequently during these conditions, leading to shorter, more fragmented drought events. In contrast, C3S-E G and C3S-E N tend to fall below the threshold in similar conditions, resulting in longer continuous drought periods, especially during winter. This sensitivity to the threshold highlights how slight model differences can have substantial effects on drought duration estimates, particularly for PV in low-generation conditions.

For the existing installed capacity scenario (Fig. 8c), the return periods mirror those of wind (Fig. 8a), due to the low levels of installed PV. In the balanced scenario (Fig. 8d), the return periods for RES droughts increase across all durations. For example, the return period for a five-day drought event, shown by the vertical dashed lines in Fig. 8, extends from roughly six months for the existing scenario, to four years for the balanced scenario in the Atlite dataset, and from about fifteen months to around five years in the two C3S-E datasets.

Across Fig. 8a, c, and, d, the return periods in the Atlite dataset are consistently higher than those in the two C3S-E datasets. For instance, in the existing scenario (Fig. 8c), an event with a one-year return period lasts six days in the Atlite dataset, compared to only five days in the C3S-E datasets. This difference underscores the importance of model selection when quantifying RES droughts, as each model's assumptions and parametrisations significantly influence drought duration estimates. Additionally, in all four panels, the similarity between results from the two C3S-E datasets suggests that assumptions in the Atlite model—such as wind turbine power curve selection and PV panel specifications—have a greater impact on RES drought duration estimates than the precise geographic distribution of RES farms when studying the return periods of RES droughts.

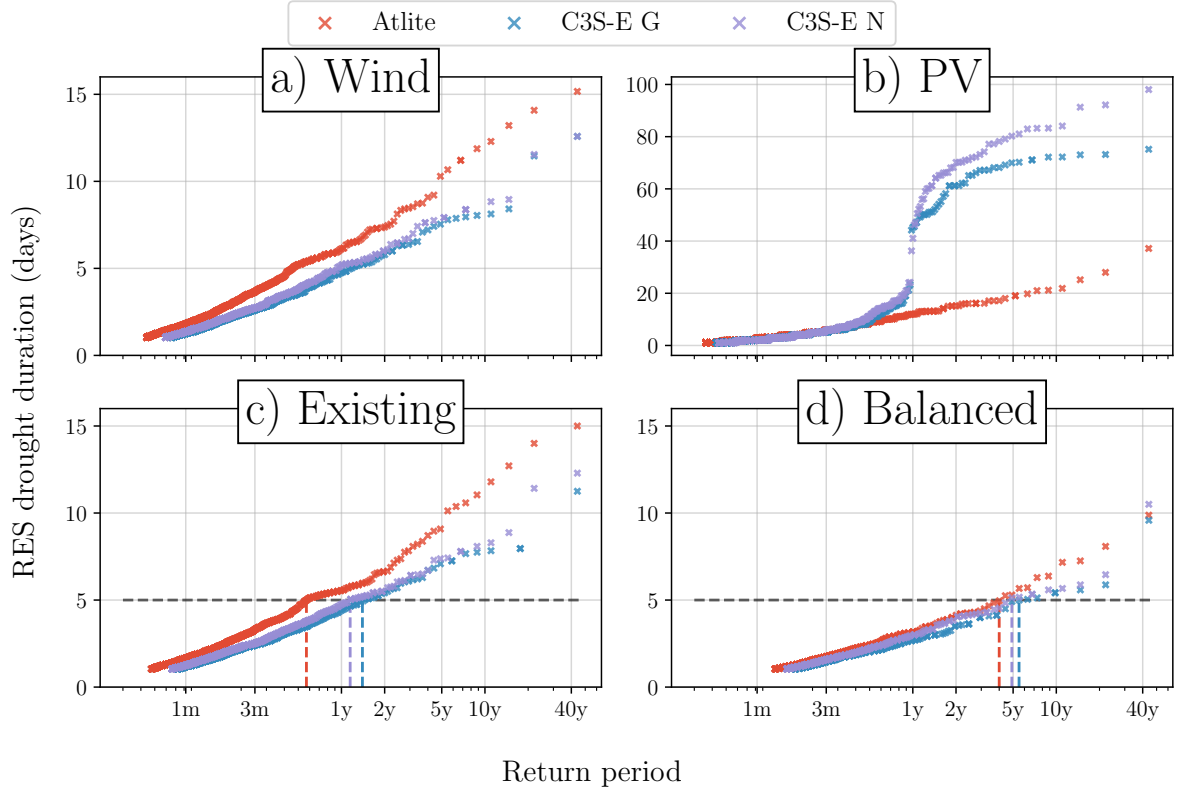


Figure 8: Return periods of the duration of RES droughts for a) Wind, b) PV, and the combination for the c) existing and d) balanced installed capacity, for Atlite (red), C3S-E G (blue), and C3S-E N (purple). The x-axis represents the return period time in a log-scale and the y-axis indicates the duration of RES drought associated with it. The horizontal dashed line in the two bottom panels marks the 5-day return period, with coloured vertical dashed marking its return period for each dataset.

4.2.3 Seasonal Distribution of RES Droughts

The seasonality of RES droughts was analysed by comparing the percentage of hours in each month classified as part of a RES drought.

For wind (Fig. 9a), RES drought percentages are higher in summer than in winter. In the Atlite dataset, for instance, an average of 24% of hours in summer (JJA) are identified as RES droughts, compared to only 4% in winter (DJF). This seasonal variation is influenced by the wind power curve model used to estimate CF, where the shape of the curve in lower wind speed regions (3-10 m/s) leads to significant differences in CF under low wind conditions. In contrast, the results for PV (Fig. 9b) show a higher percentage in winter, with RES droughts occurring over 60% of the time regardless of the dataset. The Atlite results show a higher percentage of RES drought hours for wind, and a slightly lower percentage for PV, compared to the two C3S-E datasets.

Similar to previous results, the existing installed capacity wind-PV combination (Fig. 9c) shows patterns comparable to the wind panel (Fig. 9a). However, in this panel, the number of hours classified as RES droughts in summer decreases slightly compared to the wind-only scenario. This reduction can be explained by the contribution of PV generation during the summer months in the existing scenario, even though it constitutes only 11% of total capacity. Since the number

of RES drought hours for PV in summer is near zero, this small contribution has a noticeable impact on reducing overall drought hours. In the balanced scenario (Fig. 9d), all three datasets show a reduction in monthly RES drought frequency. Annual reductions in median RES drought frequency are observed across the datasets, dropping from 14% to 5% for Atlite, from 8% to 3% for C3S-E G, and from 9% to 4% for C3S-E N. The balanced mix of wind and PV in this scenario reduces the seasonal signal overall and significantly decreases the percentage of RES drought hours in the summer. By reducing the frequency of summer droughts while maintaining resilience during winter, the balanced scenario offers a more reliable energy supply that better aligns with seasonal demand patterns.

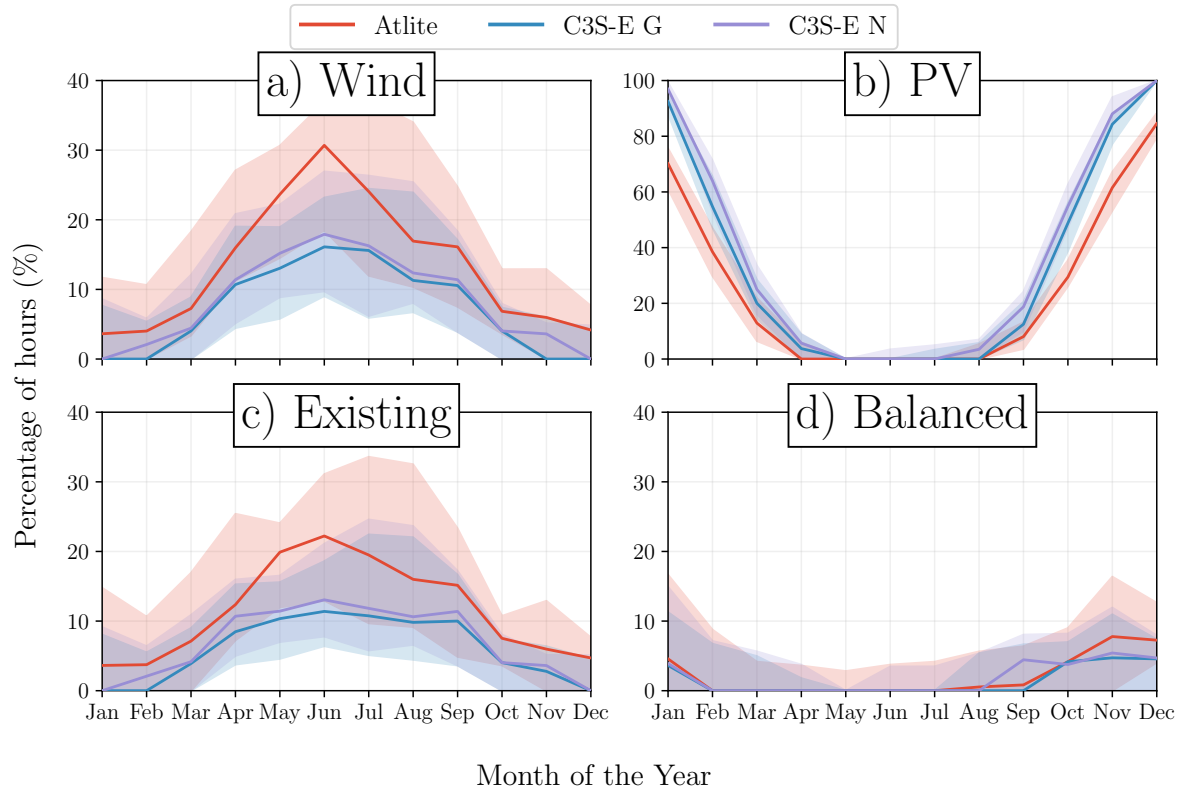


Figure 9: Percentage of hours in a month identified as a RES drought for a) Wind, b) PV, and the combination for the c) existing and d) balanced installed capacity, for Atlite (red), C3S-E G (blue), and C3S-E N (purple). The x-axis represents the month of the year, and the y-axis indicates the percentage of hours. Lines correspond to the median values and the area between the first and third quartiles is shaded.

4.2.4 Change of Threshold

In this study, a threshold CF value of 0.1 was used to identify RES droughts. To assess how sensitive the results are to this threshold, the annual number of events was calculated across a range of CF threshold values (Fig. 10).

Across all four panels, the results reveal a general trend: as the threshold increases, so does the number of identified events. This increase, however, is not uniform across datasets and energy sources, but the overall pattern remains consistent. When the threshold increases, smaller events merge into larger, less frequent events. Depending on the dataset, the number of events reaches a peak around or after a threshold of 0.2, and then gradually decreases until only a single event encompasses the entire time series.

Overall, the four panels indicate that regardless of the threshold applied, the Atlite dataset consistently identifies more events than the two C3S-E datasets, except for PV when the threshold is below 0.08. This finding suggests that Atlite, likely due to its more accurate representation of wind generation in Ireland, captures more RES drought events that might be missed with different modelling assumptions in the C3S-E datasets.

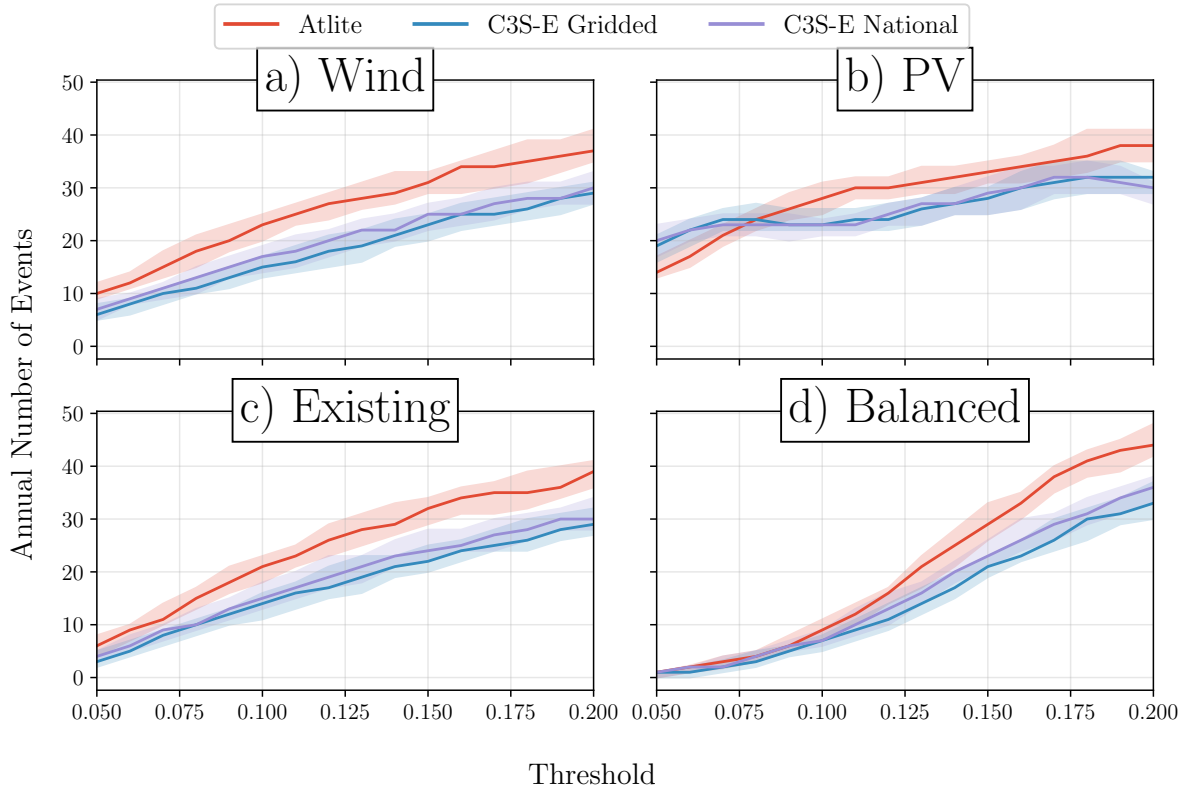


Figure 10: Number of RES drought per year for a) Wind, b) PV, and the combination for the c) existing and d) balanced installed capacity, for Atlite (red), C3S-E G (blue), and C3S-E N (purple). The x-axis represent the threshold from 0.05 to 0.2 of the CF with a 0.01 increment. The y-axis indicates the annual number of events. Each line correspond to the median value and the first and third quartiles are shown in shaded area

5 Discussion and Conclusions

This study highlighted the key differences between three RES models: Atlite, C3S-E G, and C3S-E N, in their ability to represent RES droughts. One of the most significant differences is how each dataset incorporates the specific locations of RES farms. Both Atlite and C3S-E G consider the locations of wind and PV farms, which should, in theory, provide a more accurate representation of RES generation. While this approach improves PV drought models, our analysis indicates that for wind, the Atlite dataset performs better overall, especially in its close alignment with EirGrid data for wind generation estimates. This finding suggests that although the inclusion of RES farm locations is beneficial, particularly for PV, the accuracy of the power curve model in Atlite may be the critical factor in producing realistic time series for low-generation events.

The results showed that the two C3S-E datasets (C3S-E G and C3S-E N) consistently yield similar outcomes, indicating that their methodological differences have minimal impact. In contrast, Atlite stands out for its closer alignment with EirGrid data, particularly in wind generation, as seen in the verification process (Section 4.1.1). This distinction was also evident in the analysis, where Atlite reported higher return periods and a greater number of RES droughts, especially in scenarios with a balanced share of RES. One of the study’s most critical findings is that the accuracy of RES drought modelling relies more on the precision of the wind power curve and PV panel models than on the specific locations of RES farms. Atlite’s superior performance highlights the importance of selecting accurate models for assessing RES drought risks. This careful model selection can better quantify risks, support effective planning, and avoid the potential underestimation of capacity needs, which is essential for ensuring energy security.

Looking at the balanced scenario, the analysis showed a significant improvement in the management of RES droughts due to the complementary nature of wind and PV generation. Wind and PV together perform better in terms of drought frequency and duration than either would individually, largely because of the seasonal anti-correlation between the two energy sources. This diversification reduces the seasonal impact on RES droughts, as PV generation peaks in the summer and wind generation is more consistent in winter. Ireland currently has a highly wind-dependent energy system, but with ambitious targets for PV installations in the coming years, the energy mix is expected to approach a balance between wind and PV capacity. This balanced approach offers a more stable and secure energy supply by mitigating RES drought risks. For policymakers, these findings underscore the importance of meeting these capacity targets to enhance energy security through diversification. Additionally, the choice of model for RES drought assessment becomes increasingly critical as more renewable capacity is integrated into the system.

In terms of future research, there are two main topics to explore. First, future climate data could be integrated with energy scenarios to better understand how climate change might affect RES droughts. Second, expanding the scope of the study to include Europe would provide a more comprehensive understanding of RES droughts in an interconnected energy grid. However, this expansion would require extensive verification across all EU countries, making it a more complex but highly relevant challenge.

6 Acknowledgments

7 Funding information

8 Author contribution

References

- [1] European Commission. Implementing the RePowerEU action plan: investments needs, hydrogen accelerator and achieving the bio-methane targets, May 2022. <https://eur-lex.europa.eu/legal-content/EN/TXT/?uri=SWD:2022:230:FIN> Accessed: 2024-11-06.
- [2] EuroStat. Renewable Energy Statistics, December 2023. https://ec.europa.eu/eurostat/statistics-explained/index.php?title=Renewable_energy_statistics Accessed: 2024-11-06.
- [3] Hannah C Bloomfield, David J Brayshaw, Alberto Troccoli, Clare M Goodess, Matteo De Felice, Laurent Dubus, Philip E Bett, and Yves-Marie Saint-Drenan. Quantifying the sensitivity of european power systems to energy scenarios and climate change projections. *Renewable Energy*, 164:1062–1075, February 2021.
- [4] Hannah C Bloomfield, David J Brayshaw, Len C Shaffrey, Phil J Coker, and Hazel E Thornton. Quantifying the increasing sensitivity of power systems to climate variability. *Environmental Research Letters*, 11(12):124025, 2016.
- [5] Karin van der Wiel, Laurens P. Stoop, B. R. H. Van Zuijlen, Russell Blackport, M. A. Van den Broek, and F. M. Selten. Meteorological conditions leading to extreme low variable renewable energy production and extreme high energy shortfall. *Renewable and Sustainable Energy Reviews*, 111:261–275, September 2019.
- [6] Frank Kaspar, Michael Borsche, Uwe Pfeifroth, Jörg Trentmann, Jaqueline Drücke, and Paul Becker. A climatological assessment of balancing effects and shortfall risks of photovoltaics and wind energy in germany and europe. *Advances in Science and Research*, 16:119–128, July 2019.
- [7] Masamichi Ohba, Yuki Kanno, and Daisuke Nohara. Climatology of dark doldrums in japan. *Renewable and Sustainable Energy Reviews*, 155:111927, March 2022.
- [8] Fabian Mockert, Christian M Grams, Tom Brown, and Fabian Neumann. Meteorological conditions during periods of low wind speed and insolation in Germany: The role of weather regimes. *Meteorological Applications*, 30(4):e2141, 2023.
- [9] Martin János Mayer, Bence Biró, Botond Szücs, and Attila Aszódi. Probabilistic modeling of future electricity systems with high renewable energy penetration using machine learning. *Applied Energy*, 336:120801, April 2023.
- [10] D. Raynaud, B. Hingray, B. François, and J.D. Creutin. Energy droughts from variable renewable energy sources in European climates. *Renewable Energy*, 125:578–589, 2018.
- [11] Katherine Z. Rinaldi, Jacqueline A. Dowling, Tyler H. Ruggles, Ken Caldeira, and Nathan S. Lewis. Wind and Solar Resource Droughts in California Highlight the Benefits of Long-Term Storage and Integration with the Western Interconnect. *Environmental Science and Technology*, 55(9):6214–6226, May 2021.

- [12] Anasuya Gangopadhyay, Ashwin K. Seshadri, Nathan J. Sparks, and Ralf Toumi. The role of wind-solar hybrid plants in mitigating renewable energy-droughts. *Renewable Energy*, 194:926–937, July 2022.
- [13] Sam Allen and Noelia Otero. Standardised indices to monitor energy droughts. *Renewable Energy*, 217:119206, November 2023.
- [14] Jacek Kapica, Jakub Jurasz, Fausto A. Canales, Hannah Bloomfield, Mohammed Guezgouz, Matteo De Felice, and Zbigniew Kobus. The potential impact of climate change on european renewable energy droughts. *Renewable and Sustainable Energy Reviews*, 189:114011, January 2024.
- [15] Cameron Bracken, Nathalie Voisin, Casey D. Burleyson, Allison M. Campbell, Z. Jason Hou, and Daniel Broman. Standardized benchmark of historical compound wind and solar energy droughts across the Continental United States. *Renewable Energy*, 220:119550, 2024.
- [16] Hans Hersbach, Bill Bell, Paul Berrisford, Shoji Hirahara, András Horányi, Joaquín Muñoz-Sabater, Julien Nicolas, Carole Peubey, Raluca Radu, Dinand Schepers, et al. The ERA5 global reanalysis. *Quarterly Journal of the Royal Meteorological Society*, 146(730):1999–2049, July 2020.
- [17] Copernicus Climate Change Service (C3S). Climate and energy indicators for Europe from 1979 to present derived from reanalysis., 2020. Accessed on 28-11-2024.
- [18] Laurent Dubus, Yves-Marie Saint-Drenan, Alberto Troccoli, Matteo De Felice, Yohann Moreau, Linh Ho-Tran, Clare Goodess, Rodrigo Amaro E Silva, and Luke Sanger. C3S Energy: A climate service for the provision of power supply and demand indicators for Europe based on the ERA5 reanalysis and ENTSO-E data. *Meteorological Applications*, 30(5):e2145, September 2023.
- [19] Fabian Hofmann, Johannes Hampp, Fabian Neumann, Tom Brown, and Jonas Hörsch. Atlite: a lightweight Python package for calculating renewable power potentials and time series. *Journal of Open Source Software*, 6(62):3294, 2021.
- [20] Jianling Li, Ziwen Zhao, Dan Xu, Peiquan Li, Yong Liu, Md Apel Mahmud, and Diyi Chen. The potential assessment of pump hydro energy storage to reduce renewable curtailment and co2 emissions in northwest china. *Renewable Energy*, 212:82–96, 2023.
- [21] Maximilian Parzen, Hazem Abdel-Khalek, Ekaterina Fedotova, Matin Mahmood, Martha Maria Frysztacki, Johannes Hampp, Lukas Franken, Leon Schumm, Fabian Neumann, Davide Poli, et al. Pypsa-earth. a new global open energy system optimization model demonstrated in africa. *Applied Energy*, 341:121096, 2023.
- [22] Kamran Ali Khan Niazi and Marta Victoria. Comparative analysis of photovoltaic configurations for agrivoltaic systems in europe. *Progress in Photovoltaics: Research and Applications*, 31(11):1101–1113, 2023.
- [23] EirGrid & SONI. System and Renewable Data Reports. <https://www.eirgrid.ie/grid/system-and-renewable-data-reports> Accessed: 2024-11-06.
- [24] Patrick T. Brown, David J. Farnham, and Ken Caldeira. Meteorology and climatology of historical weekly wind and solar power resource droughts over western North America in ERA5. *SN Applied Sciences*, 3(10):814, October 2021.

- [25] Noelia Otero, Olivia Martius, Sam Allen, Hannah Bloomfield, and Bettina Schaepli. Characterizing renewable energy compound events across Europe using a logistic regression-based approach. *Meteorological Applications*, 29(5):e2089, September 2022. 13.
- [26] Yves-Marie Saint-Drenan, Lucien Wald, Thierry Ranchin, Laurent Dubus, and Alberto Troccoli. An approach for the estimation of the aggregated photovoltaic power generated in several European countries from meteorological data. *Advances in Science and Research*, 15:51–62, May 2018.
- [27] Iain Staffell and Stefan Pfenninger. Using bias-corrected reanalysis to simulate current and future wind power output. *Energy*, 114:1224–1239, November 2016.
- [28] Hans G. Beyer, Gerd Heilscher, and Stefan Bofinger. A robust model for the mpp performance of different types of pv-modules applied for the performance check of grid connected systems. *Eurosun*, page 8, 2004.
- [29] EirGrid & SONI. Shaping Our Electricity Future, 2023.

Appendix